actuators

MDPI

Article

Design, Modeling, and Characteristics Analysis of Halbach Permanent Magnetic Spring

Yuexuan Lou, He Zhang * and Haoran Cai

The School of Electrical Engineering & Automation, Harbin Institute of Technology, Harbin 150001, China; 21b906040@stu.hit.edu.cn (Y.L.); 23s106129@stu.hit.edu.cn (H.C.)
* Correspondence: h.zhang@hit.edu.cn

Abstract: Magnetic springs, which can be used to replace traditional mechanical springs, have many advantages, such as necessitating no physical contact, generating no friction, no vibration or noise, and having a long lifespan. Nevertheless, their strong nonlinearity limits their widespread application. In this study, we developed a novel permanent magnet spring to address this issue: a Halbach permanent magnetic spring, with a large levitation force and an approximately linear force characteristic curve. First, we introduce the structure and the parameters of the Halbach permanent magnetic spring. Second, we describe the levitation force performance and the stiffness performance of the Halbach permanent magnetic spring using finite element analysis. Third, we analyze the trends through which different parameters influence the levitation force performance and stiffness performance. Finally, we provide recommendations for the future design of and improvement in the Halbach permanent magnetic spring.

Keywords: magnetic spring; Halbach; finite element method; characteristics analysis

Citation: Lou, Y.; Zhang, H.; Cai, H. Design, Modeling, and Characteristics Analysis of Halbach Permanent Magnetic Spring. *Actuators* **2024**, *13*, 453. https://doi.org/10.3390/act13110453

Academic Editors: Feng Sun, Zhiqiang Long, Suyuan Yu, Jin Zhou, Ran Zhou and Chuan Zhao

Received: 7 October 2024
Revised: 5 November 2024
Accepted: 11 November 2024
Published: 12 November 2024

1. Introduction

Springs, which are mechanical parts that work in several machines and devices owing to their elasticity, have many different functions, such as controlling the movement of objectives, mitigating impact, isolating vibration, storing energy, and measuring the magnitude of forces [1]. However, conventional mechanical springs often cause failures due to fatigue, fracture, and relaxation, among other metal material failures. These failures can substantially reduce equipment lifetime, performance, and safety [2]. The magnetic spring, which is a magnetic actuator consisting of permanent magnets or electromagnets that generate a magnetic force or torque, is an ideal solution to replace the classic mechanical spring [3]. Magnetic springs are simple in structure and easy to implement. Moreover, because of the lack of contact, friction, and wear between the magnetic poles, magnetic springs have extremely long lifespans and function without vibration or noise [4]. The stiffness of magnetic springs is adjustable and can even be negative [5–7]. They can even perform some jobs that classic mechanical springs cannot [8,9]. As a result of these benefits, magnetic springs have been applied in many fields. The most basic application of magnetic springs is as a substitution for mechanical springs in various suspensions to provide support force. Diez-Jimenez [10] presented a mechanical suspension integrating a passive magnetic spring and an eddy current damper. The magnetic suspension provided good mechanical properties combined with excellent cleanness and high reliability, which are desirable in mechanical systems in space applications. Tu [11] designed a negative stiffness magnetic spring by employing a couple of columnar magnets with a specific arrangement, which can be used for a semiactive seat suspension to reduce the vibration experienced by vehicle drivers. The suspension system can achieve excellent low-frequency vibration suppression. Kwac [12] showed that an X-type magnetic spring consisting of a magnet, a linear spring, and seat suspension with nonlinear characteristics was the optimal design to

increase comfort while driving. Han [13] presented an improved novel magnetic actuator model that can be applied in portable display units. Magnetic springs can also be used in actuators. Tian [14] discussed a piezoelectric vibration feeder with a magnetic spring that has a more stable resonance frequency and feeding speed within nominal loading. Olaru [15] designed a vibration electromagnetic inertial actuator based on a linearized magnetic spring. The device, mounted on a mechanical structure, generated vibration forces higher than 4 N in the frequency range of 70 divided by 500 Hz. Rodriguez-Leon [16] found that the use of magnetic springs with actuators may reduce the energy consumption of robots performing trajectories due to the high-hardness magnetic properties of their energy storage.

Magnetic springs can be divided into permanent magnetic and electrical exciting springs according to how the magnetic force is generated [17,18]. Permanent magnet springs are superior to electrical exciting springs in terms of energy loss and waste heat. However, permanent magnet springs have a severe drawback: the magnetic force rapidly and nonlinearly decreases with increasing displacement [19,20]. Although the nonlinear characteristic of a magnetic spring is required in some devices, this problem directly restricts the widespread use of permanent magnet springs as an alternative to mechanical springs and may act as a hurdle to control systems [21,22].

This article presents a novel permanent magnetic spring, named the Halbach permanent magnetic spring (HPMS), that solves the above-mentioned problem. The approximately linear relationship between the levitation force and displacement makes it more applicable for replacing classical mechanical springs. The HPMS provides a large levitation force to carry heavy loads. The unparalleled levitation force without contact allows HMPSs to be used as support for metrology frames of lithography machines and some other large and heavy ultraprecision equipment. Additionally, an HPMS is fully capable of working in a vacuum environment. The absence of physical contact with the outside world provides favorable conditions for the isolation of vibrations and disturbances. Its nearly linear mechanical characteristics also facilitate the design of active vibration isolation systems. Most space equipment requires support or levitation devices on Earth to simulate the microgravity environment of space for testing to ensure that the equipment can properly operate in space. Traditional ground test equipment is usually supported by hydraulic or rope suspension. However, because of the physical contact between the ground test equipment and the object under testing, this type of support often creates coupling, which directly affects the accuracy of the test results. However, HMPSs create none of these challenges. The near-linear mechanical characteristics of HMPSs can be used to design and fabricate a more versatile ground test platform.

First, the structure and geometrical parameters of the HPMS are described in detail. Second, the mechanical properties of the HPMS, the relationship between the levitation force and the stiffness with the vertical displacement are studied using finite element analysis. The two advantages of the HPMS are supported by the data. To facilitate the use and design of the HPMS, we provide a characteristics analysis to demonstrate the influence of different parameters on the performance.

2. Structure and Performance

2.1. Structure

The proposed HPMS has a bilateral topology. Its structure, which contains a stator and a mover, is shown in Figure 1, and its specific configuration is shown in Table 1.

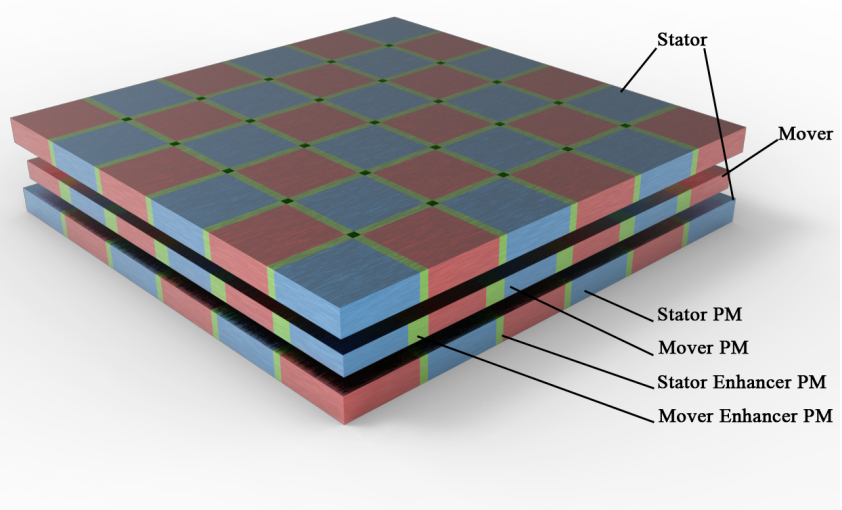

Figure 1. Structure of Halbach permanent magnetic spring.

Table 1. Specifications of Halbach permanent magnetic spring.

Parameter	Value	Unit
length	232	mm
Width	232	mm
Height	47	mm
Material	N35	-
Work Direction	Vertical Direction (z)	-
Maximum Displacement	±2	mm
Target Force	9800	N
Target Stiffness	900	N/mm

The stator has two layers, which are called the upper and lower stator layers. The one layer in the mover is located in between the upper and lower stator layers. All three layers are arranged to form a Halbach Magnet Array.

The two kinds of permanent magnets (PMs) in the HPMS are vertically magnetized PMs, used to generate a primary magnetic field, and horizontally magnetized PMs, which are located between the vertically magnetized PMs. These PMs are named stator enhancer PMs and mover enhancer PMs, respectively. All the layers consist of thirty-six stator or mover PMs and sixty enhancer PMs.

Each of the stator or mover PMs has the opposite magnetization direction to its neighboring PM in the same layer. Each mover PM's magnetization aligns with the upper stator PM and opposes the lower stator PM below it. The magnetization direction of both the stator enhancer PMs and the mover enhancer PMs are explicitly determined according to the magnetic field reinforcement direction of the Halbach permanent arrays.

The Halbach permanent magnet array can simultaneously reinforce one side of its magnetic field and weaken the other side. To increase the levitation force of the HPMS, both the upper and lower stator should be set as the state that strengthens the magnetic field near the mover. The reinforcement side of the mover should be chosen based on the HPMS's specific application requirements, as shown in Figure 2. If the mover reinforces its upper side magnetic field, the HPMS will work as a tension spring with a nearly constant positive stiffness when the displacement of the mover progressively shifts from negative to positive. In contrast, the HPMS will have negative stiffness when the mover reinforces its lower side magnetic field.

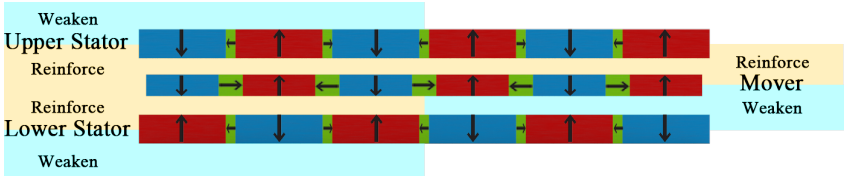

Figure 2. Magnetic field reinforcement area of each layer.

The proposed HPMS can generate more levitation force than normal magnetic springs because of the following: First, each one of the mover PMs is simultaneously attracted by the stator PM directly above and is repelled by the stator PM directly below. Second, the use of permanent magnet arrays can use the levitation force of every mover PM and reduce the end effect of the magnetic field. Finally, the use of the Halbach array can reinforce the internal magnetic field of the HPMS.

2.2. Parameters

Like other actuators, the HPMS needs two types of parameters to specify its structure: positioning and geometric parameters.

The positioning parameters of the HPMS include the positioning parameters between the layers and those within each layer. Because the HPMS only works in the vertical direction, the stators and mover are aligned on the horizontal surface. l, which is the distance in the vertical direction between the inner side of the stators and the mover, is enough to describe the relationships between the different layers. For the positioning parameters within each layer, only one parameter, called p, is needed to control the distance between two adjacent PMs in the same layer.

Both kinds of PMs in the HPMS are needed to determine the geometric size in the three dimensions of the Cartesian coordinates. We used PPFF, which is the parameter that can conveniently change the horizontal size of the PMs when p is changed, in this study. It is the ratio of the width or length of the PMs to p. Only one PPFF is required for the stator and mover PMs due to their square horizontal cross-section. The length PPFF and the width PPFF are necessary for the enhancer PMs. In contrast with the horizontal parameters, the PM thickness is directly described in millimeters. The main parameters are shown in Figure 3.

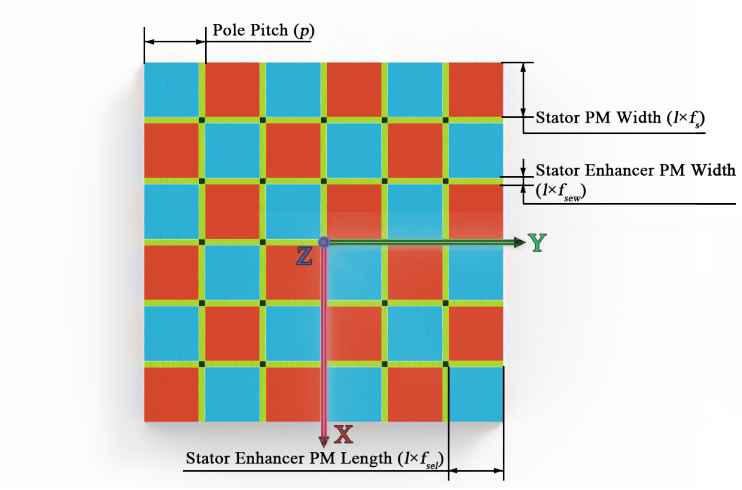

(**a**) Top view

Figure 3. *Cont.*

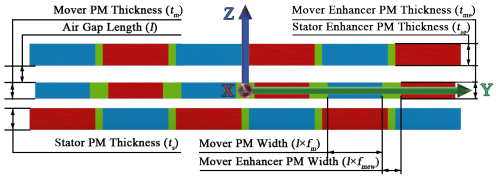

(**b**) Side view

Figure 3. Parameters of Halbach permanent magnetic spring.

2.3. Magnetic Field Distribution

To validate the effectiveness of the Halbach array, we analyzed the magnetic flux density distribution in the HPMS, as shown in Figure 4. In Figure 4a, the left side shows an elevated view of the upper stator layer, while the right side presents a top view of the lower stator layer. These two are in a vertically symmetrical relationship within the HPMS. It can be observed that the magnetic field in the upper stator layer is stronger than that in the lower stator layer, thus demonstrating that the Halbach array in the mover layer, as shown in Figure 2, has successfully enhanced the upper magnetic field while weakening the lower magnetic field. Simultaneously, the magnetic flux density distribution in the same horizontal plane is relatively uniform, which contributes to the HPMS's stable operation. Figure 4b illustrates the HPMS's cross-sectional magnetic flux density distribution perpendicular to the *X*-axis. To improve visibility, we added the air region to this subfig. From this figure, it can be observed that all three Halbach arrays are effective, as evidenced by the stronger magnetic fields on the stator layers' inner sides and the mover layer's upper side compared to their opposite sides. This validates the effectiveness of our HPMS design as presented in Figure 2.

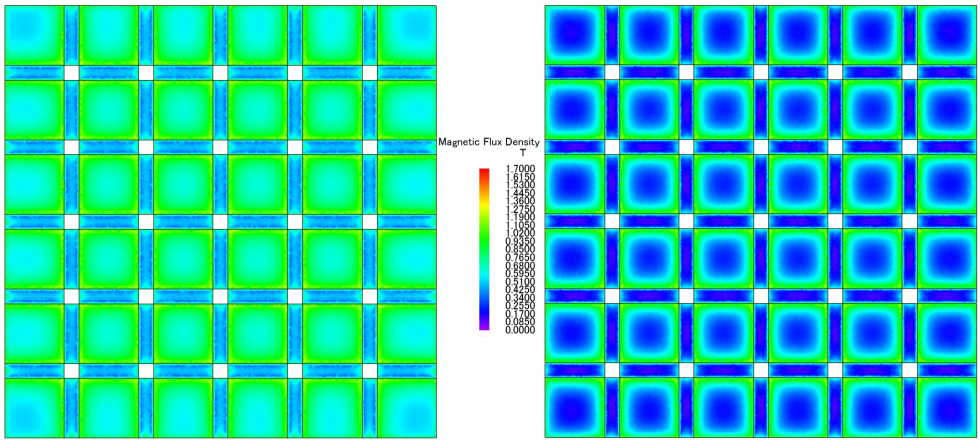

(**a**)

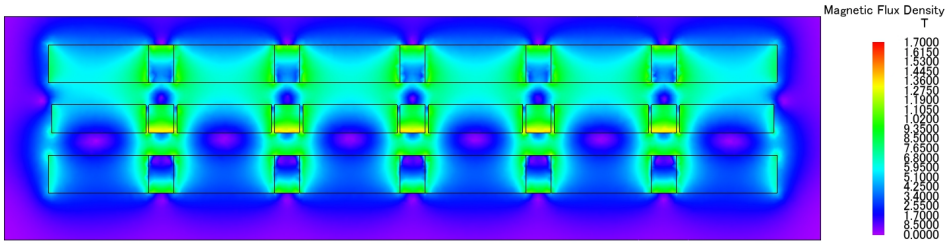

(**b**)

Figure 4. Magnetic field distribution of the Halbach permanent magnetic spring. (**a**) An elevated view of the upper stator layer and top view of the lower stator layer; (**b**) a sectional view.

2.4. Performance

We used JMAG® ver 22.1, a finite element analysis software developed in Japan, to simulate the performance of the HPMS. Subsequently, the equivalent magnetic charge method was employed to validate the influence trends obtained from the FEM.

For the FEM, the model's geometry replicated the designed HPMS, with initial parameter values as specified in the study. The PMs' material properties were based on N35 NdFeB, with its BH curve at 20 °C incorporated into the model. Boundary conditions were addressed by creating a sufficiently large air region around the HPMS to ensure accurate levitation force calculations. Meshing strategies involved separate meshes for the PM group and the surrounding air region, with mesh sizes manually set for each. Convergence criteria were established for both linear and nonlinear calculations, employing the incomplete Cholesky conjugate gradient method for linear equations and the Newton–Raphson method for nonlinear iterations. The convergence tolerance was set to 1×10^{-8} for linear solvers and 1×10^{-3} for nonlinear calculations.

For the equivalent magnetic charge method, the PM's magnetization can be effectively represented by two equivalent magnetic charge surfaces aligned with the magnetization direction. The surface density of these equivalent magnetic charges is given by:

$$\sigma_m = \mu_0 M_r = B_r$$

The total magnetic field intensity can be expressed as:

$$\overrightarrow{H} = \frac{1}{4\pi} \oiint_S \frac{\sigma_m(\overrightarrow{r} - \overrightarrow{r'})}{\left|\overrightarrow{r} - \overrightarrow{r'}\right|^3} \, \mathrm{d}S$$

where $\overrightarrow{r}$ is the observation point; $\overrightarrow{r'}$ is the source point.

Upon the evaluation of the integral in the equation, we derive the magnetic flux density. The interaction force between PM1 and PM2 can be directly determined using the Lorentz force formula.

$$F(\vec{x}) = \frac{\mu_0 B_{r1} B_{r2}}{4\pi} \sum_{i=0}^{1} \sum_{j=0}^{1} \sum_{k=0}^{1} \sum_{l=0}^{1} \sum_{m=0}^{1} \sum_{n=0}^{1} (-1)^{i+j+k+l+m+n} \vec{\varepsilon}(u, v, w)$$

where: $u = \alpha - (-1)^i a_1 + (-1)^j a_2$; $v = \beta - (-1)^k b_1 + (-1)^l b_2$; $w = \gamma - (-1)^m c_1 + (-1)^n c_2$; $r = \sqrt{u^2 + v^2 + w^2}$.

When PM1 and PM2 are both magnetized along the z-axis, the components of $\vec{\varepsilon}$ are given by:

$$\varepsilon_x = \frac{1}{2}(v^2 - w^2)\log(r - u) + uv\log(r - v) + vw \arctan\frac{uv}{wr} + \frac{1}{2}ur$$

$$\varepsilon_y = \frac{1}{2}(u^2 - w^2)\log(r - v) + uv\log(r - u) + uw \arctan\frac{uv}{wr} + \frac{1}{2}vr$$

$$\varepsilon_z = -uw\log(r - u) - vw\log(r - v) + uv \arctan\frac{uv}{wr} - wr$$

The two advantages of the HPMS are its large levitation force and improved stiffness. For all PMs in this study, we used NdFeB grade N35 as an example. The results presented in Figures 5 and 6 correspond to Scheme A of the HPMS parameters as specified in Scheme A of Table 2. Given that our designed HPMS primarily operates in the vertical direction, and the horizontal forces are extremely small and cannot be analyzed, we focus our analysis solely on the HPMS's vertical performance. The calculated data prove the advantages of the HPMS.

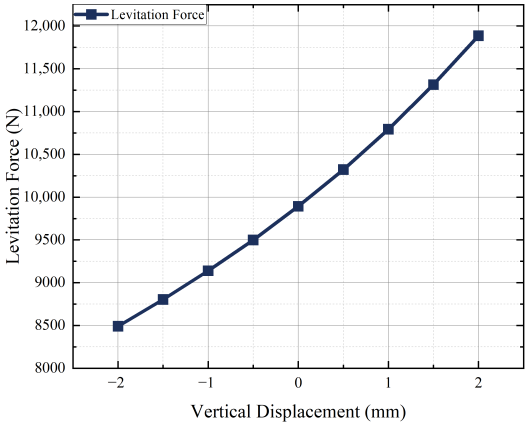

Figure 5. Levitation force performance of Halbach permanent magnetic spring.

Table 2. The initial values of the parameters and their specific ranges of change.

Parameter/Dimension Unit	Scheme A	Scheme B	Range	Step
Air Gap Length (l)/mm	7	10	[2.5, 12.5]	1
Pole Pitch (p)/mm	40	36	[30, 50]	1
Stator PM PPFF (f_s)	0.8	0.7	[0.6, 0.8]	0.02
Mover PM PPFF (f_m)	0.75	0.62	[0.6, 0.8]	0.02
Stator PM Thickness (t_s)/mm	12	14	[9.5, 14.5]	0.5
Mover PM Thickness (t_m)/mm	9	10	[6.5, 11.5]	0.5
Stator Enhancer PM Length PPFF (f_{sel})	0.8	0.76	[0.6, 0.8]	0.02
Mover Enhancer PM Length PPFF (f_{mel})	0.75	0.63	[0.55, 0.75]	0.02
Stator Enhancer PM Width PPFF (f_{sew})	0.2	0.18	[0.04, 0.2]	0.02
Mover Enhancer PM Width PPFF (f_{mew})	0.2	0.12	[0.04, 0.2]	0.02
Stator Enhancer PM Thickness (t_{se})/mm	12	10.5	[7, 12]	0.5
Mover Enhancer PM Thickness (t_{me})/mm	9	7	[4, 9]	0.5

As shown in Figure 5, the relationship between the levitation force of the HPMS and the vertical displacement is extremely close to linear and relatively similar to that of mechanical springs. This trait, which is lacking in most magnet springs, allows the HPMS to replace traditional mechanical springs. The HPMS can also reduce the workload of developing control systems by regarding this function in Figure 5 as linear. This means that the HPMS has better stiffness performance, as shown in Figure 6.

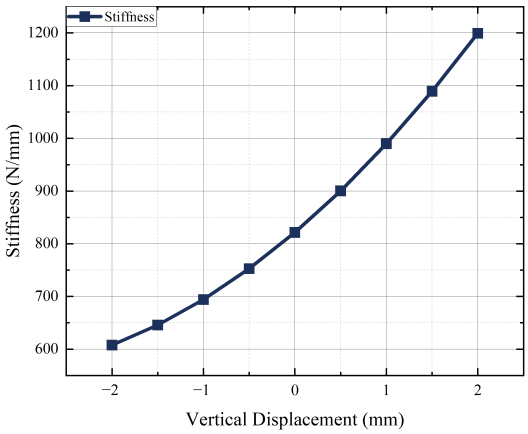

Figure 6. Stiffness performance of Halbach permanent magnetic spring.

A large levitation force can be generated by the HPMS according to the zero displacement point, as shown in Figure 5. This large levitation force can be generated to adapt to heavy-load working conditions by expanding the size of the permanent magnet arrays in

the HPMS. Due to the Halbach arrays, the HPMS can provide a stronger force than regular magnetic springs, even when they are identical in volume.

To further demonstrate the advantages of the HPMS, we compared the levitation force performance of another large-load magnetic device with that of the HPMS. For its specific topology, please refer to the literature [23]. To ensure the reasonableness and validity of the comparison, the total volume, number of major PMs, and geometry of the major PMs were the same for both. We calculated the levitation force performance of another large-load magnetic device using JMAG in a similar setup, as shown in Figure 7.

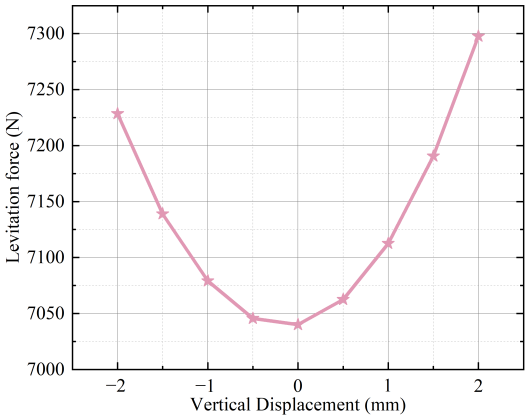

Figure 7. Levitation force performance of another large-load magnetic device.

Comparing Figure 7 with Figure 5, we found that the HPMS still had a higher levitation force at the same total volume. Compared with the topology of the other method [23], the initial position levitation force of the HPMS is approximately 40.5% higher. This is further proof of the large levitation force produced by the HPMS.

The shape of the curve in Figure 7 is a parabolic line. This also reflects the strong nonlinearity of the magnetic force between the PMs with respect to the displacement. The curve for the HPMS is different: its nearly linear levitation force performance curve is unparalleled by other topologies.

Other magnetic springs reported in the literature [1,5–7,9–11,17,22], for example, do not have the advantages provided by the HPMS. We will not repeat the above analysis for these other springs. Their levitation forces are much smaller than that of the HPMS and they do not have nearly linear levitation force performance.

3. Characteristics Analysis

As shown in Section 2.2, the Halbach permanent magnet arrays in the magnetic spring are so complex that many parameters are needed to determine the unique topology. This substantially hinders the design of the magnetic spring. Finding an optimization result in an optimal design of the HPMS will be challenging if all twelve parameters are regarded as the design variables that require optimizing. Determining which parameter should be adjusted and by how much when a particular HPMS performance is required would be difficult. Therefore, we analyzed the trends and the weights of the influence of each parameter on the performances of the HPMS.

We also studied the influences of each parameter on the levitation force performance and stiffness performance through the finite element method using JMAG®. When we adjusted only one parameter, as shown in Table 2, the other parameters remained at their initial value and were not changed to show the relationship between the performance and this parameter. First, we used the finite element analysis software to calculate the levitation force on the mover of the HPMS under these parameters when the vertical displacement varied from −2 to 2 mm in 0.5 mm steps. Second, we performed a third-order polynomial fitting to the levitation force data. We obtained the stiffness data under the specific parameter through a derivative computation on the fitting data. Finally, after we

separately collected the levitation force and stiffness data in the vertical displacement of 0 mm, we obtained the characteristics analysis results, which are shown in Figure 8.

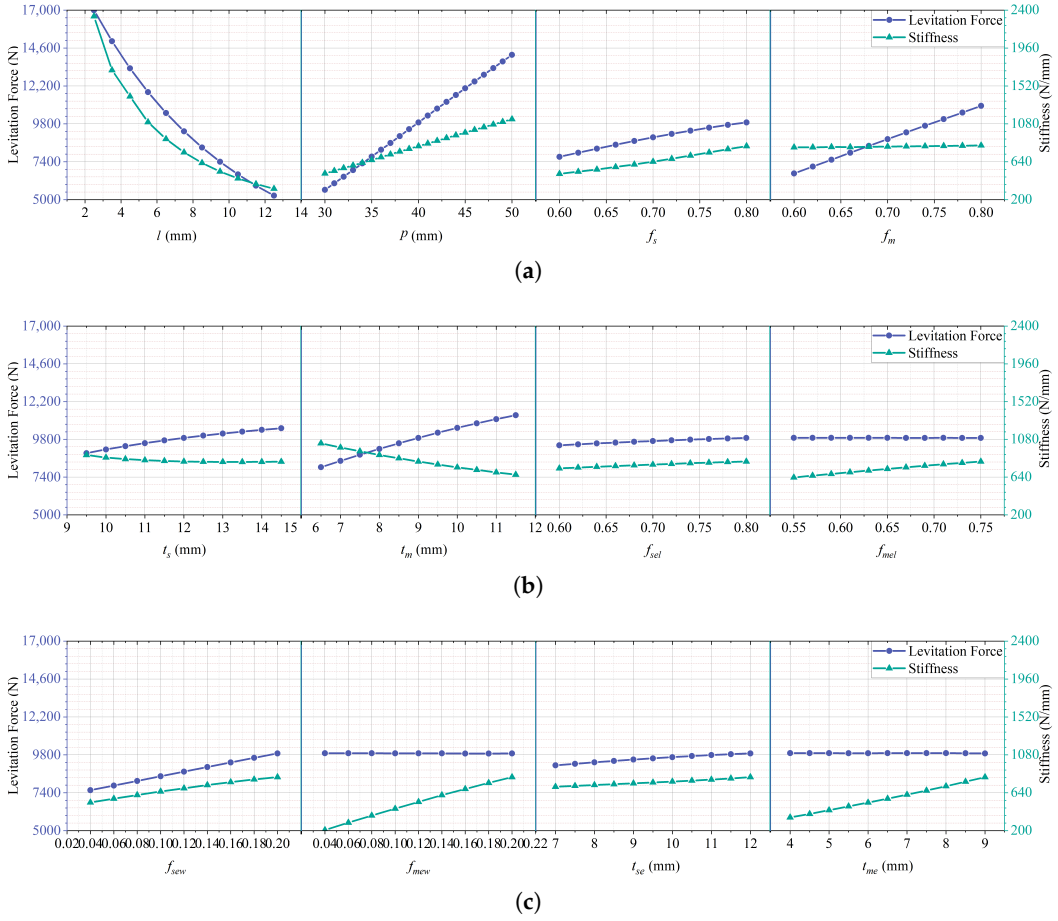

Figure 8. Results of the characteristics analysis for each parameter. (**a**) l, p, f_s, and f_m; (**b**) t_s, t_m, f_{sel}, and f_{mel}; (**c**) f_{sew}, f_{mew}, t_{se}, and t_{me}.

4. Discussion

We discussed and analyzed the results of the characteristics to determine the trends through which the different parameters influence the performance of the HPMS, and their weights. Consequently, we determined constructive recommendations for the design and modification of HMPSs in the future.

4.1. Effects of Dimensional Parameters on Performance

We described and studied the influence trends of each parameter on the levitation force and stiffness performance of the HPMS one at a time.

For l, levitation force and stiffness rapidly decrease with the progressive increase in l. Both decrease from 16,994.99 to 5257.86 N and 2328.48 N/mm to 326.72 N/mm, respectively. The rate of descent gradually slows as l increases. The large curvature of the lines also implies that l is a critical parameter in the regulation of the levitation forces and stiffness of an HPMS.

Increases in p can simultaneously linearly increase the levitation force and stiffness. The levitation force increases from 5620.57 to 14,171.71 N, and the stiffness increases from 504.40 N/mm to 1134.47 N/mm. Both of their rates of increase are almost constant and relatively fast. The nearly linear influence of p enables the quantitative adjustment of HPMS performance.

The increases in the PPFFs of stator and mover PMs lead to increases in the levitation force and stiffness. For f_s, the levitation force increases from 7712.91 to 9892.63 N, and the

stiffness increases from 500.57 to 821.37 N/mm. The growth rate of the levitation force gradually grows; however, the growth rate of the stiffness slowly decreases. The level of change in these rates is not particularly significant. For f_m, the levitation force increases from 6662.00 to 10,944.34 N. The variation in rate is not obvious. The shape of the curve is similar to a straight line. Therefore, increases in stiffness are not obvious from 807.48 to 829.56 N/mm. The amount of change in stiffness can be neglected in this situation. It follows that f_m is more suitable than the stator PM PPFF if only the levitation force of the HPMS needs to be adjusted.

The influence trends of t_s and t_m are similar. Increases in thickness cause an increase in levitation force and a decrease in stiffness. For t_s, the levitation force increases from 8921.74 to 10,506.67 N, and the stiffness decreases from 896.96 to 816.17 N/mm. For t_m, the levitation force increases from 8031.23 to 11,338.92 N, and the stiffness decreases from 1034.28 to 668.40 N/mm. The main difference between the two trends is the degree of curvature of the curves. The trends of t_s show relatively strong nonlinearity. The rates of variation in the levitation force and stiffness both progressively slow. In contrast, the trends in t_m influence are essentially approximately linear. Therefore, the geometric parameters of t_m are more suitable for HPMS performance adjustment than those of t_s.

The influence trends of f_{sel} and f_{mel} on the stiffness are somewhat alike. Both show a linear growth rule with increased enhancer PM length PPFF. For f_{sel}, the range is 741.81 to 821.37 N/mm. For f_{mel}, the range is 635.38 to 821.37 N/mm. Nevertheless, we noted a discrepancy in the influence trends of the two parameters on the levitation force. An increase in f_{sel} results in an increase in levitation force. However, the rate of increase is slightly slower. The range is 9424.98 to 9892.63 N. Conversely, the increase in f_{mel} causes a fluctuating decrease in levitation force. The range is 9898.21 to 9892.63 N.

The effect of f_{sew} on the levitation force performance is more analogous to that on the stiffness. The increasing pattern of both is approximately linear. The range of levitation force varies from 7561.48 to 9892.63 N. The range of stiffness varies from 527.34 to 821.37 N/mm. Yet, the stiffness curve is slightly more curved than the levitation force curve. The effect of f_{mew} on the performance of the HPMS dramatically varies. The levitation force is not sensitive to changes in f_{mew} change. However, the variation in stiffness is approximately linear, ranging from 207.55 to 821.37 N/mm.

Figure 9 shows the levitation force performance curve of the HPMS when f_{mew} is 0.04. In this parabolic curve, the minimum levitation force occurs at the vertical displacement of −1.5 mm, which is 9749.73 N. In this case, the HPMS no longer has the advantage described above, which is that the relationship between the levitation force of the HPMS and the vertical displacement is extremely close to linear. Hence, f_{mew} strongly influences the curvature degree and shape of the levitation force performance curve. Excessively crooked curves can also lead to drastic changes in HPMS stiffness. The other parameters that control the geometry of the mover enhancer PM, including f_{mel} and t_{me}, have a comparable effect. Figure 9 provides a more severe case used to facilitate explanation. The linearity of the levitation performance curve of the HPMS can only be guaranteed if the mover enhancer PM geometry is carefully sized at the beginning of the design. Nevertheless, when modifying an existing HPMS, changing the geometry of the mover enhancer PM is likely to lead to a bending of the levitation performance curve, which will deteriorate the performance of the HPMS.

The influence trend of enhancer PM thickness is almost identical to that of the enhancer PM width PPFF. However, for stator enhancer PM thickness, the bending directions of the levitation force curve and the stiffness curve do not coincide. As stator enhancer PM thickness increases, the growth rate of the levitation force gradually slows, while that of the stiffness gradually increases. The adjustment of t_{me} is consistent with that of f_{mew}. The range of the levitation force varies from 9912.93 to 9892.63 N. The variation range of stiffness varies from 353.90 to 821.37 N/mm.

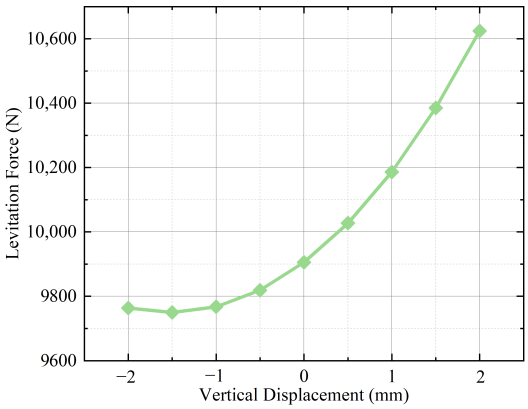

Figure 9. Distortions in levitation force performance of HPMS.

4.2. Parameter Weights

To compare the weights of the different parameters, we set the same upper bound, lower bound, and division for the axes of levitation force and stiffness in Figure 8. Observing the relationship between the various subplots in Figure 8, we found that the range in the vertical axis occupied by the curves of different parameters is wide. This phenomenon implies that each parameter's capacity to impact the HPMS force performance and stiffness performance differs. To facilitate the comparison of different parameters' influence, we define Parameter Weights in this study as the percentage ratio of two quantities calculated at zero displacement. The numerator is the range of variation in the HPMS's levitation force or stiffness when a single parameter is changed. The denominator is the initial levitation force or stiffness value using the scheme parameters specified in Table 2. Figure 10 illustrates the weights of all 12 parameters. The results labeled "Scheme A by FEM" in this figure correspond to the curves presented in Figure 8.

In general, of twelve parameters of the HPMS, the two most influential are as follows: l is ranked first, with the strongest impact on the performance. The 10 mm variation in l in Figure 8 results in 11,737.13 N and 2001.76 N/mm for levitation force and stiffness, respectively. This influence of this parameter is incomparable to that of the other parameters. The second is p, which has a different law of influence than l. When p produces a shift of 20 mm, the changes in levitation force and stiffness are 8551.14 N and 630.07 N/mm, respectively, which are slightly smaller than those of l. The remaining ten parameters do not have the same weights as these two parameters.

Figure 10 shows that, in general, the geometrical parameters of the PMs, which generate the central part of the working magnetic field, have a stronger capacity to influence the levitation force than those of enhancer PMs. However, the geometric parameters of enhancer PMs have more substantial weight in terms of stiffness than those of stator PMs and mover PMs. Additionally, the effect of mover PMs on the levitation force is generally stronger than that of stator PMs. f_m beneficially affects the magnitude of the HPMS levitation force due to its minimal impact on the levitation force. Although the parameters of mover enhancer PMs almost exclusively affect stiffness, they can only be used in the beginning stages of design and do not apply to modifications afterward. The specific reasons are explained in Figure 9, above.

For Scheme A, presented in Table 2, we employed both the FEM and MM for analysis. As illustrated in Figure 10, the results from these two approaches show close agreement, with minimal discrepancies, thereby validating the effectiveness of the FEM. To ensure that Scheme A was not an isolated case, we selected Scheme B from Table 2, which has entirely different parameters, and subjected it to MM analysis. Scheme B exhibits a markedly different levitation force of 4182.3 N (according to MM results), in contrast to Scheme A. And, Figure 10 reveals that Scheme B follows patterns similar to those observed in Scheme A. This consistency underscores the broad applicability of the trends identified through the characteristics analysis. These findings collectively reinforce the robustness of our

analysis across diverse parametric configurations, lending credence to the generalizability of our results.

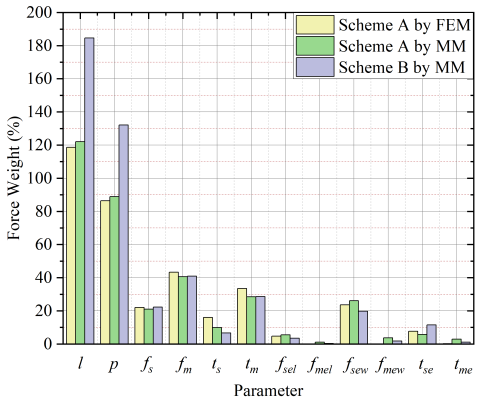

(**a**)

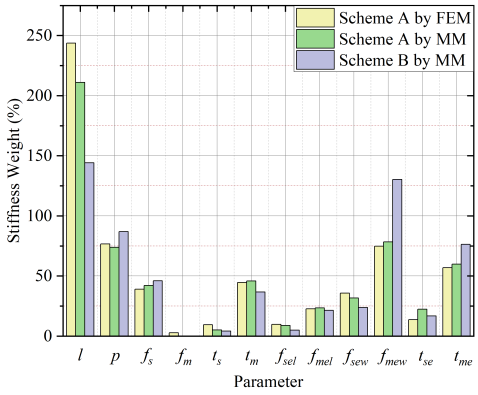

(**b**)

Figure 10. Parameter weights. (**a**) Force weight; (**b**) Stiffness weight.

4.3. Recommendations for Design and Modification

Considering the possible quantitative performance requirements for HPMSs, we discuss two prominent cases: design and modification.

When a new HPMS needs to be designed, the air gap is the first parameter that needs to be determined, owing to it having the strongest influence and strong nonlinearity. Then, p needs to be determined, depending on the approximate range of the target levitation force and stiffness. Once these parameters are confirmed, the PM geometry in the HPMS needs to be determined. The value of the levitation force can be further specified by altering stator and mover PMs. The size of mover enhancer PMs strongly influences the stiffness and needs to be fixed before the other geometrical dimensions. Moreover, to ensure the mechanical performance of the HPMS, these parameters should be modified as little as possible once they are determined.

The process of modifying an existing HMPSs may widely differ from the designed one. For instance, altering parameters with nonlinear influence trends, such as the air gap, should be avoided. To protect the levitation performance of the HPMS, the dimensions of the mover enhancer PMs should likewise be unchanged. Given the lack of other qualifications, the HPMS levitation force should be regulated alone by using f_m. However, the stiffness of the HPMS is challenging to adjust with only a single parameter: it requires the action of several parameters in conjunction.

In addition, if an optimization design is required, the parameters with higher weights should be selected as design variables to set the optimization objectives.

5. Conclusions

We designed a novel permanent magnet spring, an HPMS, in this study. It has a more proximate linear force characteristic curve and greater levitation force than classic permanent magnet springs and is a better alternative to conventional mechanical springs. Furthermore, we acquired the variation in the curves of the levitation force and the stiffness of the HPMS with the vertical displacement of the mover by using finite element analysis. We analyzed the characteristics of the parameters that are essential to determining the specific structure of the HPMS. We obtained the influence trends of each parameter on the performance and their weights. Based on the results of the characteristics analysis, we provided further guiding recommendations for the HPMS for future designs and modifications.

Author Contributions: Writing—original draft preparation, Y.L.; writing—review and editing, H.Z.; conceptualization, H.C. All authors have read and agreed to the published version of the manuscript.

Funding: This research was funded by the National Natural Science Foundation of China, grant number 52377044.

Institutional Review Board Statement: Not applicable.

Informed Consent Statement: Not applicable.

Data Availability Statement: The data presented in this study are available on request from the corresponding author.

Acknowledgments: The authors thank the anonymous reviewers for providing critical comments and suggestions that improved the manuscript.

Conflicts of Interest: The authors declare no conflicts of interest. The funders had no role in the design of the study; in the collection, analyses, or interpretation of data; in the writing of the manuscript; or in the decision to publish the results.

Abbreviations

The following abbreviations are used in this manuscript:

HPMS	Halbach permanent magnetic spring
PM	Permanent magnet
FEM	Finite Element Method
MM	Mathematical Modeling
PPFF	Pole Pitch Filling Factor

References

1. Sun, F.; Zhang, M.; Jin, J.J.; Duan, Z.Y.; Jin, J.Q.; Zhang, X.Y. Mechanical analysis of a three-degree of freedom same-stiffness permanent magnetic spring. *Int. J. Appl. Electromagn. Mech.* **2016**, *52*, 667–675. [CrossRef]
2. Mrak, B.; Lenaerts, B.; Driesen, W.; Desmet, W. Optimal magnetic spring for compliant actuation-validated torque density benchmark. *Actuators* **2019**, *8*, 18. [CrossRef]
3. Mrak, B.; Wex, B.; Mitterhofer, H. Methodology for shape optimization of magnetic designs: Magnetic spring characteristic tailored to application needs. *Actuators* **2022**, *11*, 37. [CrossRef]
4. Qiu, Y.; Zhu, Y.P.; Luo, Z.; Gao, Y.; Li, Y.Q. The analysis and design of nonlinear vibration isolators under both displacement and force excitations. *Arch. Appl. Mech.* **2021**, *91*, 2159–2178. [CrossRef]
5. Yang, T.; Cao, Q.J. Modeling and analysis of a novel multi-directional micro-vibration isolator with spring suspension struts. *Arch. Appl. Mech.* **2022**, *92*, 801–819. [CrossRef]
6. Zhou, Z.H.; Chen, S.H.; Xia, D.; He, J.J.; Zhang, P. The design of negative stiffness spring for precision vibration isolation using axially magnetized permanent magnet rings. *J. Vib. Control* **2019**, *25*, 2667–2677. [CrossRef]
7. Cheng, C.; Ma, R.; Hu, Y.; Wang, W.P. Performance analysis of a quasi-zero-stiffness vibration isolator with time-delayed dual feedback control. *Arch. Appl. Mech.* **2022**, *92*, 4017–4032. [CrossRef]
8. Forbrigger, C.; Schonewille, A.; Diller, E. Tailored Magnetic Torsion Springs for Miniature Magnetic Robots. In Proceedings of the IEEE International Conference on Robotics and Automation, Xi'an, China, 30 May–5 June 2021. [CrossRef]
9. Woodward, M.A.; Sitti, M. Universal Custom Complex Magnetic Spring Design Methodology. *IEEE Trans. Magn.* **2018**, *54*, 1–13. [CrossRef]

10. Diez-Jimenez, E.; Alen-Cordero, C.; Alcover-Sanchez, R.; Corral-Abad, E. Modelling and test of an integrated magnetic spring-eddy current damper for space applications. *Actuators* **2021**, *10*, 8. [CrossRef]
11. Tu, L.X.; Ning, D.H.; Sun, S.S.; Li, W.X.; Huang, H.; Dong, M.M.; Du, H.P. A novel negative stiffness magnetic spring design for vehicle seat suspension system. *Mechatronics* **2020**, *68*, 102370. [CrossRef]
12. Kwac, L.K.; Kim, H.G.; Song, J.S.; Shin, H.J.; Kim, B.J.; An, K.H.; Hye-min, L. Optimal design and performance evaluation of X-type magnetic spring suspension for commercial vehicle seat. *J. Korean Soc. Manuf. Technol. Eng.* **2014**, *23*, 456–464.
13. Han, I. Analysis of novel magnetic-spring actuators for portable units. *Trans. KSME* **2004**, *28*, 1942–1949.
14. Tian, X.C.; Yang, Z.G.; Liu, Y.; Shen, Y.H.; Chen, S. Structural design and experimental analysis of a piezoelectric vibration feeder with a magnetic spring. *Micromachines* **2014**, *5*, 547–557. [CrossRef]
15. Olaru, R.; Mihai, M.M.; Girtan, B.; Petrescu, C.; Arcire, A. Design and experiment of an electromagnetic vibrational inertial actuator using linearized magnetic spring. *Rev. Roum. Sci. Tech.-Ser. Electrotech.* **2019**, *63*, 253–258.
16. Rodriguez-Leon, J.F.; Cervantes, I.; Castillo-Castaneda, E.; Carbone, G.; Cafolla, D. Design and preliminary testing of a magnetic spring as an energy-storing system for reduced power consumption of a humanoid arm. *Actuators* **2021**, *10*, 136. [CrossRef]
17. Olaru, R.; Arcire, A.; Petrescu, C.; Mihai, M.M.; Girtan, B. A novel vibration actuator based on active magnetic spring. *Sens. Actuator A-Phys.* **2017**, *264*, 11–17. [CrossRef]
18. Woodward, M.A.; Sitti, M. Tailored magnetic springs for shape-memory alloy actuated mechanisms in miniature robots. *IEEE Trans. Robot.* **2020**, *35*, 589–601. [CrossRef]
19. Lee, S.; Hirata, K.; Kato, M. Intrinsic localized mode in a multiple mass dynamic vibration systems using non-linear magnetic springs. *IEEJ Trans. Electr. Electron. Eng.* **2022**, *17*, 13–18. [CrossRef]
20. Ahamed, R.; Howard, I.; McKee, K. Study of gravitational force effects, magnetic restoring forces, and coefficients of the magnetic spring-based non-linear oscillator system. *IEEE Trans. Magn.* **2022**, *58*, 1–18. [CrossRef]
21. Yao, G.C.; Huang, W.C. Performance of a guideway seismic isolator with magnetic springs for precision machinery. *Earthq. Eng. Struct. Dyn.* **2009**, *38*, 181–203. [CrossRef]
22. Wang, W.; Wei, H.T.; Wei, Z.H. Numerical analysis of a magnetic-spring-based piecewise non-linear electromagnetic energy harvester. *Eur. Phys. J. Plus* **2021**, *137*, 56. [CrossRef]
23. Zhang, H.; Lou, Y.X.; Zhou, L.S.; Kou, Z.Q.; Mu, J.R. Modeling and Optimization of a Large-Load Magnetic Levitation Gravity Compensator. *IEEE Trans. Ind. Electron.* **2023**, *70*, 5055–5064. [CrossRef]